pISSN 1229-3008 eISSN 2287-6251
Progress in Superconductivity and Cryogenics
Vol.23, No.4, (2021), pp.30~34 https://doi.org/10.9714/psac.2020.23.4.030

Electromagnetic design study of a 7 T 320 mm high-temperature superconducting MRI magnet with multi-width technique incorporated

Won Seok Jang, Geonyoung Kim, Kibum Choi, Jeonghwan Park, Jeseok Bang, and Seungyong Hahn*

Seoul National University, Seoul, Korea

(Received 19 November 2021; revised or reviewed 20 December 2021; accepted 21 December 2021)

Abstract

Superconducting magnets have paved the way for opening new horizons in designing an electromagnet of a high field magnetic resonance imaging (MRI) device. In the first phase of the superconducting MRI magnet era, low-temperature superconductor (LTS) has played a key role in constructing the main magnet of an MRI device. The highest magnetic resonance (MR) field of 11.7 T was indeed reached using LTS, which is generated by the well-known Iseult project. However, as the limit of current carrying capacity and mechanical robustness under a high field environment is revealed, it is widely believed that commercial LTS wires would be challenging to manufacture a high field (>10 T) MRI magnet. As a result, high-temperature superconductor together with the conducting cooling approach has been spotlighted as a promising alternative to the conventional LTS. In 2020, the Korean government launched a national project to develop an HTS magnet for a high field MRI magnet as an extent of this interest. We have performed a design study of a 7 T 320 mm winding bore HTS MRI magnet, which may be the ultimate goal of this project. Thus, in this paper, design study results are provided. Electromagnetic design and analysis were performed considering the requirements of central magnetic field and spatial field uniformity.

Keywords: high-field MRI, MRI magnet, no-insulation winding technique

1. INTRODUCTION

Since the first discovery of nuclear magnetic resonance (NMR) imaging in the 1970s, magnetic resonance imaging (MRI) has played a key role in the medical and biochemical discipline. As a result, MRI is widely used in hospitals and clinics for medical diagnosis since it can provide pictures of the anatomy and the physiological processes. The key advantage of the MRI technique is better contrast in medical images, compared to other medical imaging techniques, such as computed tomography. However, the improvement of image contrast is still a major concern.

Strong magnetic fields are required in order to obtain high-quality MR images with better contrast since they can substantially improve the signal-to-noise ratio as well as the consequent spatial and temporal resolution of medical images. Therefore, superconducting magnets generating high fields far beyond 1 T have been considered an indispensable option for the main magnet of an MRI system. In the early stage of superconducting MRI main magnet development, low-temperature superconductors (LTS), such as Nb_3Sn and NbTi, have been widely adopted to fabricate the main magnet [1]. However, the use of high-temperature superconductor (HTS) has been in the spotlight recently as a promising option [2]. Furthermore, no-insulation (NI) technique which makes turn-to-turn insulation unnecessary enhanced the stability of the magnet compared to the LTS magnet [3-13]. As a result, national R&D project to develop 6 T 320 mm All- REBa2Cu3O7-x (REBCO, RE = rare earth) MRI magnet embarked in 2020. A collaborative team led by SuperGenics Co., Ltd., has conducted a comparative study of superconducting MRI magnets.

In this paper, we present the electromagnetic analysis results of the 7 T 320 mm winding bore HTS superconducting MRI magnet design with field homogeneity of 111 ppm at 12 cm diameter of spherical volume (DSV). No-insulation (NI), multi-width winding techniques and inner notch approach were applied to achieve the design goal. This design is an alternative to that of the metal-insulation (MI) design for the main project.

2. MAGNET DESIGN

2.1. Conceptual design of a 7 T 320 mm MRI magnet

2.1.1. Conductor and magnet configuration

Major design requirements of the magnet were (1) a central magnetic field of 7 T, (2) homogeneity at 12 cm diameter of spherical volume (DSV) below 200 ppm.

The design constraints of the magnet were (1) magnet inner radius of 160 mm, (2) identical magnet outer radius for all DP coils for ease of DP-DP splicing [14], (3) tape per single pancake (SP) under 200 m not to use splice joint, and (4) total conductor length below 40 km.

* Corresponding author: hahnsy@snu.ac.kr

TABLE I
KEY PARAMETERS OF REBCO CONDUCTORS.

Parameter	Unit	Value
Width	[mm]	4.1, 5.1, 6.1
Conductor thickness	[mm]	0.14
Cu stabilizer thickness	[mm]	0.04 (0.02 per side)
Substrate thickness	[mm]	0.1

The magnet is comprised of a stack of double pancake (DP) coils wound with REBCO tapes. The key parameters of the conductors are summarized in Table I. The tapes with different widths of 4.1 mm, 5.1 mm, and 6.1 mm were used in the magnet. NI winding technique was applied to construct the DP coils.

The cross-section image of the upper half of the solenoidal-shaped magnet is shown in Fig. 1. The magnet consists of 91 NI DPs wound with various widths of conductors. A 'module (M)' denotes a set of DP coils having the same tape width. "4", "5", "6", "C", and "N" represent DP coils wound with REBCO tapes of 4.1mm width (4), 5.1mm width (5), 6.1mm width (6), located at the center (Center), and with inner notch design applied (Notch). Notched coils have a smaller number of turns per pancake to have the same outer radius as other coils.

Table II shows the key parameters of the magnet. The overall height is 927.4 mm. A 0.2 mm thickness insulation sheet was used as a pancake-to-pancake spacer in a DP coil, while two 0.5 mm thickness spacers were put in between DP coils. The total 4.1 mm equivalent conductor requirement is 38.2 km. The key operation parameters of the magnet are illustrated in Table III.

2.1.2. Design strategy: multi-width and inner notch design

DP coils are conventionally wound with the HTS tapes of the same width [15-17]. However, the multi-width technique was applied to increase the operating current as improving the minimum value of the field-dependent critical current in the magnet. Therefore, the decrease of critical current density at the coils at the top region due to the strong radial magnetic field applied perpendicular to the tapes can be offset by widening the tapes.

Inner notch design was applied to 2nd to 12th DP coils from the z=0 to improve the field homogeneity.

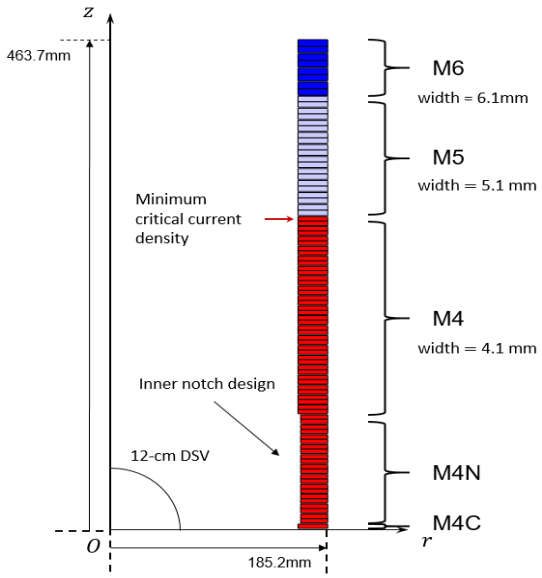

Fig. 1. Cross-section image of the magnet design (only the upper half part of the magnet). M4, M5, and M6 represent DP coils wound with REBCO tapes of 4.1mm, 5.1mm, and 6.1mm width respectively. The minimum critical current density of 191.1 A occurred at the upper single pancakes (SP) coil of the 32nd DP coil. 12 cm DSV was considered to measure the magnetic field homogeneity.

2.2. Electromagnetic analysis

2.2.1. Magnetic field calculation

The performances of the magnet were simulated by FEM. The key parameters of the magnet are shown in TABLE III. Fig. 2(a) shows the current density distribution on the upper half of the magnet in its full operation at I_{op}; Fig. 2(b) and 2(c) show the corresponding axial and radial magnetic field distribution. The magnet inductance was calculated to be 109.68 H, with a total magnetic energy of 1.1 MJ. The engineering current densities (J_e) at I_{op} are 288.4, 231.9, and 193.9 A/mm^2 for M4-M6 modules respectively.

2.2.2. Stability analysis

The measured critical current data of HTS tape depending on the magnitude and angle of the applied magnetic field and temperature were provided by SuNAM [19].

TABLE II
KEY PARAMETERS OF THE MAGNET CONFIGURATION.

Parameter	Unit	M4C	M4N	M4	M5	M6
PC spacer	[mm]			0.2		
DP-DP spacer	[mm]			0.5×2		
Inner radius, a_1	[mm]	160.0	162.1	160.0	160.0	160.0
Outer radius, a_2	[mm]			185.2		
z_{bot}	[mm]	0	4.7	108.1	296.1	410.1
z_{top}	[mm]	4.7	108.1	296.1	410.1	463.7
Overall height	[mm]			927.4		
Total conductor per module	[km]	0.19×2	3.96×2	7.81×2	4.85×2	2.30×2
Overall conductor requirement	[km]			38.2		

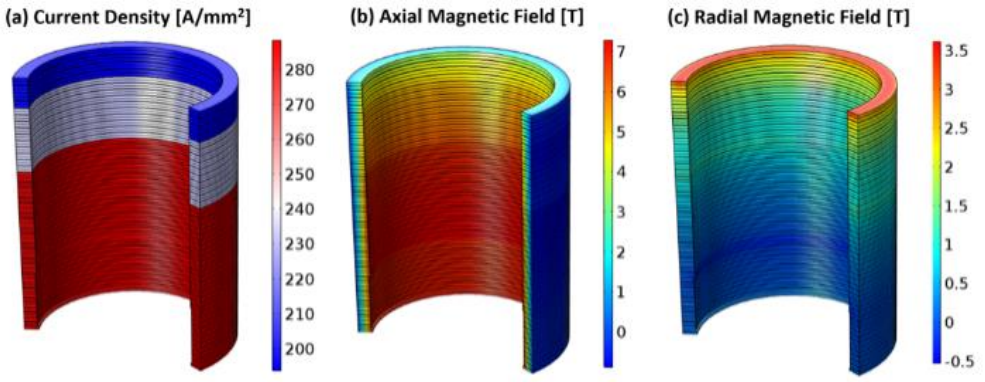

Fig. 2. (a) current density distribution (b) axial magnetic field (c) radial magnetic field of the upper half of the magnet in its full operation at operating current of 165.55 A.

TABLE III
KEY PARAMETERS OF MAGNET OPERATION.

Parameter	Unit	Value
Center field	[T]	7
Operating current, I_{op}	[A]	165.55
Critical current at 10 K, coil-field	[A]	191.1
Operating temperature	[K]	10
Self-inductance	[H]	109.7
Stored energy at 7 T	[MJ]	1.1
Contact resistivity, R_{ct}	[μΩcm^2]	40
Characteristic resistance, R_c	[mΩ]	27.1
Time constant, τ_c	[min]	68
Magnet constant	[mT/A]	42.3
Index, n		41

The minimum critical current density occurred at the upper single pancake (SP) coil of the 32nd DP coil from the midplane. The load line of the upper single pancake (SP) coil of the 32nd DP coil is shown in Fig. 3 and it is confirmed that the magnet can operate at a central magnetic field of 7 T with a critical current margin of 7.4%. The temperature margin is calculated to be 4.5 K.

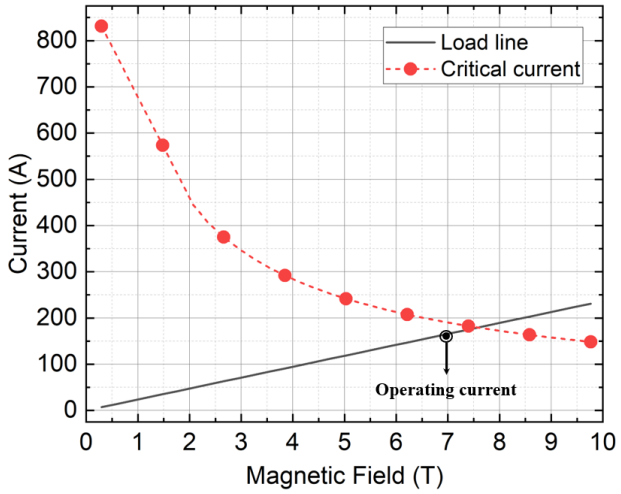

Fig. 3. The critical current of the magnet versus magnetic field with the load line for the magnet when the operating current is 165.55 A. The critical current value and its margin is 178.7 A and 7.4% respectively.

2.2.3. Lumped circuit analysis

NI HTS magnet can be presented as an equivalent circuit model where the index value is defined to characterize the property of NI HTS coils [20]. The time constant is calculated from the differential equations by the lumped circuit model represented in Fig. 4. In this circuit model, each single pancake coil is represented by self-inductance L, mutual inductance M, characteristics resistance R_c, and so-called 'index' resistance R_θ with the n-value assumed to be 41 [21]. Contact resistivity was assumed to be 40 μΩcm^2 [22]. Consisting of 182 single pancake coils, the whole magnet is described as an equivalent circuit with the single pancake coils connected in series.

Fig. 5 shows charging simulation analysis results of the magnet with a ramping-rate of 5 mA/s. Although it takes 9 hours to reach the operating current of 165.55 A due to the charging delay of NI coils, it takes 15 hours to reach the center field to 7 T.

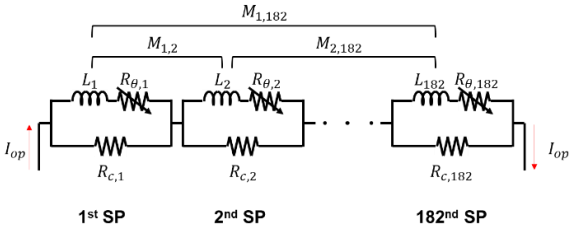

Fig. 4. Lumped circuit model of a stack of 91 NI DP coils.

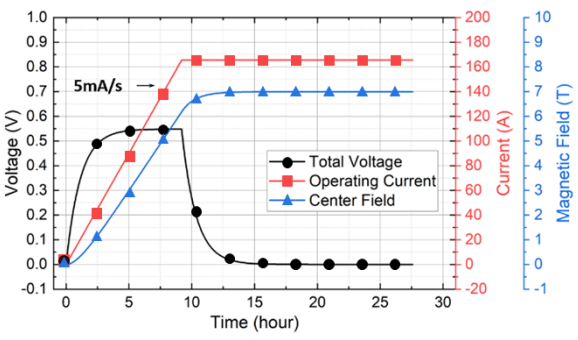

Fig. 5. Charging analysis results of the magnet with a ramping rate of 5 mA/s. Although it takes 9 hours to reach the operating current of 165.55 A, it takes 15 hours to reach the center field to 7 T.

2.2.4. Harmonic analysis

In spherical coordinate, the magnetic field near the center can be organized by using associate Legendre polynomials by the given equation:

$$B_z = \sum_{n=0}^{\infty} \sum_{m=0}^{m=n} r^n P_n^m(\cos\theta)[A_n^m \cos m\phi + B_n^m \sin m\phi], \quad (1)$$

where $r, \theta,$ and ϕ represent radial distance, polar angle, and azimuthal angle. This equation is applied to each single pancake coil respectively. Then, the magnetic field of the magnet is calculated by the superposition of all single pancake coils. Since the magnet is axis-symmetric, the terms with $m = 0$ only remain. Then, B_n^m components vanish, while A_n^0 can be calculated by [23]

$$A_n^0 = \frac{\mu_0 J U_{n+1}}{2(n+1)}, \quad (2)$$

$$U_{n+1} = \int_{b_1}^{b_2} \int_{a_1}^{a_2} \frac{\sin\theta}{r^{n+1}} P_{n+1}^1(\cos\theta) d\rho dz, \quad (3)$$

Field gradient is the rather preferred term for NMR/MRI engineers, and the conversion relation between n^{th} zonal field gradient (Z_n) and the harmonic coefficient is given by

$$Z_n = (n+1)A_n^0. \quad (4)$$

Field homogeneity at 12 cm DSV is evaluated by

$$\frac{\Delta B}{B} = \frac{B_{max} - B_{min}}{B_{max} + B_{min}}, \quad (5)$$

where B_{max}, B_{min} are maximum and minimum magnetic fields at 12 cm DSV. Table IV shows the zonal field gradients. The bracketed value in the table represents field homogeneity in units of ppm when the corresponding field gradient only exists. In detail, field homogeneity of Z_n field gradient is evaluated by Eq. (5), where the magnetic field distribution of Z_n gradient is calculated by considering only Z_n and Z_0 in Eq. (1). Dominant field gradient is Z_4 gradient with 128.5 ppm, while Z_{10} gradient is marginal.

Fig. 6 shows the comparison of field homogeneity between the magnet design with and without the inner notch design applied. The result became approximately 30 times better after the inner notch design was applied. Furthermore, the 5-gauss stray magnetic field line for the MRI magnet is represented in Fig. 7. When MRI system is installed, the magnetic field is typically suggested to not exceed 5 gauss outside the scanning suite [1]. 5-gauss line of 4.4 (R) x 6 m (Z) was calculated.

TABLE IV
ZONAL FIELD GRADIENTS OF THE MAGNETIC FIELD.

Parameter	Unit	Value
Z_2	[T/m^2] ([ppm])	7.20×10^{-2} (83.4)
Z_4	[T/m^4] ([ppm])	-1.94×10^{1} (128.5)
Z_6	[T/m^6] ([ppm])	-7.11×10^{2} (23.5)
Z_8	[T/m^8] ([ppm])	2.10×10^{4} (3.2)
Z_{10}	[T/m^{10}] ([ppm])	-4.17×10^{5} (0.3)

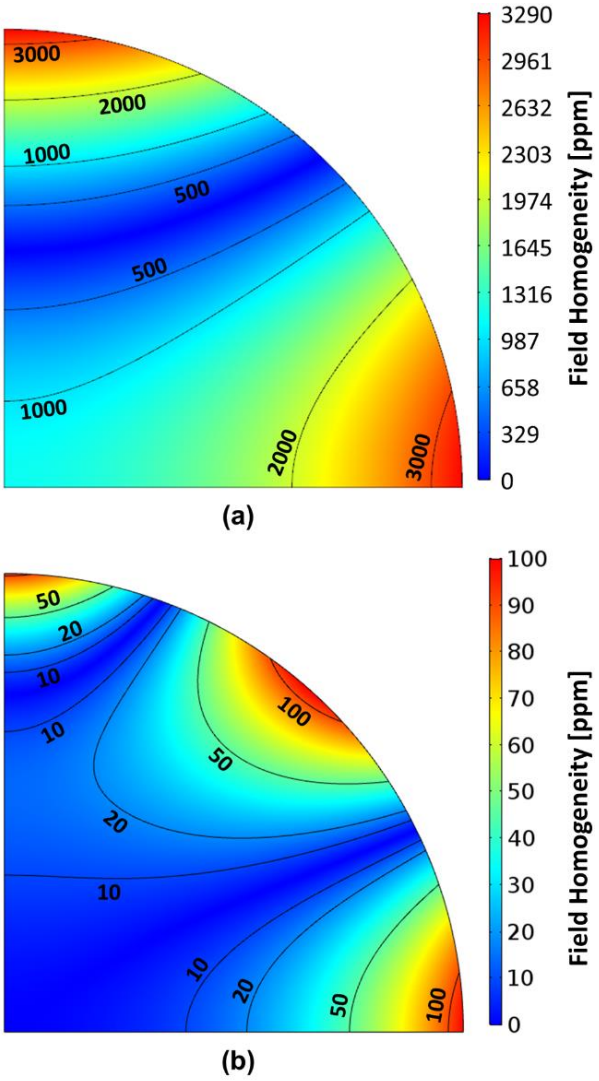

Fig. 6. Magnetic field homogeneity contour plot (a) without notch design and (b) with notch design. 12 cm DSV is represented as a quartile circle on the first quadrant of the RZ plane due to symmetry. Homogeneity is 111 ppm when the notch design was adopted.

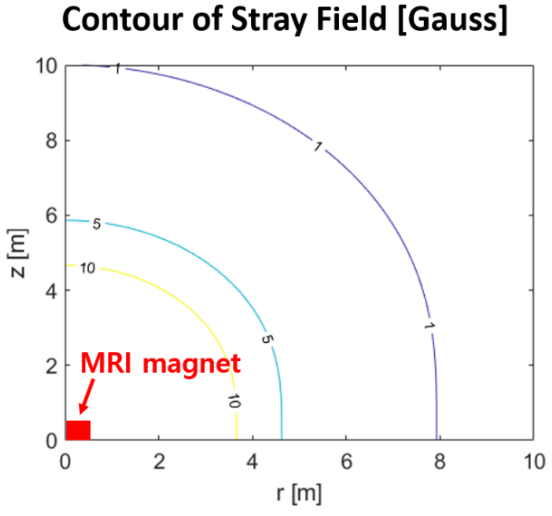

Fig. 7. The contour line plot of a 5-gauss stray magnetic field.

3. CONCLUSION

In this paper, we present a design of a 7 T 320 mm high temperature superconducting (HTS) no-insulation (NI) magnetic resonance imaging (MRI) magnet. The magnet consists of a stack of 91 NI pancake coils, and the total height of the magnet is 937.4 mm. Multi-width and notch configurations are incorporated to minimize conductor usage and improve field homogeneity. As a result, the magnet is designed to generate 7 T center field with a total conductor usage in terms of 4.1 mm width tape is 38.2 km. The magnet is designed to generate a 7 T center field, of which (2) field homogeneity of 111 ppm over 120 cm DSV with a dominant Z4 gradient. Detailed electromagnetic analysis results are as the followings: (1) load line margin of 7.4%; (2) dominant harmonic component of Z4 gradient; and (3) 5 gauss line of 4.4 (R) x 6 m (Z). Using the lumped circuit model, the total charging time is calculated to be 15 hours. Finally, this design is an alternative to the previous design for the main project.

Future design analyses including screening current analysis, quench analysis, and mechanical behavior need to be conducted for further development of a 7 T high-temperature superconducting MRI magnet.

ACKNOWLEDGMENT

This work was supported by the Korea Medical Device Development Fund grant funded by the Korea government (the Ministry of Science and ICT, the Ministry of Trade, Industry and Energy, the Ministry of Health & Welfare, the Ministry of Food and Drug Safety) (Project Number: 1711138068, KMDF_PR_20200901_0063).

REFERENCES

[1] T. Cosmus and M. Parizh, "Advances in whole-body MRI magnets," *IEEE Trans. Appl. Supercond*., vol. 21, no. 3, pp. 2104-2109, 2011.

[2] Y. Iwasa, J. Bascunan, S. Hahn, M. Tomita, and W. Yao, "High-temperature superconducting magnets for NMR and MRI: R&D activities at the MIT francis bitter magnet laboratory," *IEEE Trans. Appl. Supercond.*, vol. 20, no. 3, pp. 718-721, 2010.

[3] S. Hahn, D. Park, K. Kim, J. Bascunan, and Y. Iwasa, "No-insulation (NI) winding technique for premature-quench-free NbTi MRI magnets," *IEEE Trans. Appl. Supercond*., vol. 22, no. 3, pp. 4501004, 2012.

[4] X. Wang, S. Hahn, Y. Kim, J. Bascunan, J. Voccio, H. Lee, and Y. Iwasa, "Turn-to-turn contact characteristics for an equivalent circuit model of no-insulation ReBCO pancake coil," *Supercond. Sci. Technol*., vol. 26, pp. 035012, 2013.

[5] Y. Choi, S. Hahn, J. Song, D. Yang, and H. Lee, "Partial insulation of GdBCO single pancake coils for protection-free HTS power applications," *Supercond. Sci. Technol*., vol. 24, pp. 125013, 2011.

[6] Y. Choi, D. Kim, and S. Hahn, "Progress on the development of a 5 T HTS insert magnet for GHz class NMR applications," *IEEE Trans. Appl. Supercond*., vol. 21, no. 3, pp. 1644-1648, 2011.

[7] Y. Kim, S. Hahn, K. Kim, O. Kwon, and H. Lee, "Investigation of HTS racetrack coil without turn-to-turn insulation for superconducting rotating machines," *IEEE Trans. Appl. Supercond*., vol. 22, no. 3, pp. 5200604, 2012.

[8] S. Choi, H. Jo, Y. Hwang, S. Hahn, and T. Ko, "A study on the no insulation winding method of the HTS coil," *IEEE Trans. Appl. Supercond*., vol. 22, no. 3, pp. 4904604, 2012.

[9] Y. Choi, K. Kim, O. Kwon, J. Kang, T. Ko, and H. Lee, "The effects of partial insulation winding on the charge–discharge rate and magnetic field loss phenomena of GdBCO coated conductor coils," *Supercond. Sci. Technol*., vol. 25, pp. 105001, 2012.

[10] S. Kim, A. Saito, T. Kaneko, J. Joo, J. Jo, Y. Han, and H. Jeong, "The characteristics of the normal-zone propagation of the HTS coils with inserted Cu tape instead of electrical insulation," *IEEE Trans. Appl. Supercond*., vol. 22, no. 3, pp. 4701504, 2012.

[11] S. Hahn, Y. Kim, J. Ling, J. Voccio, D. Park, J. Bascunan, H. Shin, H. Lee, and Y. Iwasa, "No-Insulation coil under time-varying condition: magnetic coupling with external coil," *IEEE Trans. Appl. Supercond*., vol. 23, no. 3, pp. 4601705, 2012.

[12] S. Yoon, K. Cheon, H. Lee, S. Moon, I. Ham, Y. Kim, S. Park, H. Joo, K. Choi, and G. Hong, "Fabrication and characterization of 3-T/102-mm RT bore magnet using 2nd generation (2G) HTS wire with conducting cooling method," *IEEE Trans. Appl. Supercond*., vol. 23, no. 3, pp. 4600604, 2012.

[13] S. Kim, T. Kaneko, H. Kajikawa, J. Joo, J. Jo, Y. Han, and H. Jeong, "The transient stability of HTS coils with and without the insulation and with the insulation being replaced by brass tape," *IEEE Trans. Appl. Supercond*., vol. 23, no. 3, pp. 7100204, 2012.

[14] J. Kim, Y. Kim, S. Yoon, K. Shin, J. Lee, J. Jung, J. Lee, J. Kim, D. Kim, J. Yoo, H. Lee, S. Moon, and S. Hahn, "Design, construction, and operation of an 18 T 70 mm no-insulation (RE)Ba2Cu3O7-x magnet for an axion haloscope experiment," *Rev. Sci. Instruments.*, vol. 91, no. 2, pp. 023314, 2020.

[15] M. Daibo, S. Fujita, M. Haraguchi, Y. Iijima, M. Itho, and T. Saitoh, "Development of a 5T 2G HTS magnet with a 20-cm-diameter bore," *IEEE Trans. Appl. Supercond*., vol. 23, no. 3, pp. 4602004, 2013.

[16] S. Hahn, J. Bascunan, E. Bobrov, W.Kim, M. Ahn, and Y. Iwasa, "Operation and performance analyses of 350 and 700 MHz low-/high-temperature superconductor nuclear magnetic resonance magnets: A march toward operating frequencies above 1 GHz," *J. Appl. Phys*., vol. 105, pp. 024501, 2009.

[17] B. Parkinson, R. Slade, M. Mallett, and V. Chamritski, "Development of a cryogen free 1.5 T YBCO HTS magnet for MRI," *IEEE Trans. Appl. Supercond*., vol. 23, no. 3, pp. 4400405, 2012

[18] K. Bhattarai, K. Kim, S. Kim, S. Lee, and S. Hahn, "Quench analysis of a multiwidth no-insulation 7-T 78-mm REBCO magnet," *IEEE Trans. Appl. Supercond*., vol. 27, no. 4, pp. 4603505, 2017.

[19] S. Wimbush and N. Strickland, Critical current characterization of SuNAM SAN04200 2G HTS superconducting wire. [Online]. Available: https://doi.org/10.6084/m9.figshare.5182354.v1

[20] K. Bhattarai, K. Kim, K. Kim, K. Radcliff, X. Hu, C. Im, T. Painter, I. Dixon, D. Larbalestier, and S. Lee, "Understanding quench in no-insulation (NI) REBCO magnets through experiments and simulations," *Supercond. Sci. Technol*., vol. 33, pp. 035002, 2020.

[21] K. Tsuchi, A. Kikuchi, A. Terashima, K. Norimoto, M. Uchida, M. Tadawa, M. Masuzawa, N.Ohuchi, X. Wang, T. Takao, and S. Fujita, "Critical current measurement of commercial REBCO conductors at 4.2K," *Cryogenics*., vol. 85, 2017.

[22] X. Wang, S. Hahn, Y. Kim, J. Bascunan, J. Voccio, H. Lee, and Y. Iwasa, "Turn-to-turn contact characteristics for an equivalent circuit model of no-insulation ReBCO pancake coil," *Supercond. Sci. Technol*., vol. 26, pp. 035012, 2013.

[23] S. Noguchi, "Formulation of the spherical harmonic coefficients of the entire magnetic field components generated by magnetic moment and current for shimming," *J. Appl. Phys.*, vol. 115, no. 16, pp. 163908, 2014.